applied sciences

MDPI

Article

Analyzing Cutting Temperature in Hard-Turning Technique with Standard Inserts Through Both Simulation and Experimental Investigations

Pham Minh Duc *, Le Hieu Giang and Van Thuc Nguyen

Faculty of Mechanical Engineering, Ho Chi Minh City University of Technology and Education, Ho Chi Minh City 700000, Vietnam; gianglh@hcmute.edu.vn (L.H.G.); nvthuc@hcmute.edu.vn (V.T.N.)
* Correspondence: ducpm@hcmute.edu.vn

Abstract: The cutting temperature in hard turning is extremely high, which reduces tool life, lowers machined-surface quality, and affects dimensional control. However, hard turning differs greatly from conventional turning in that the cutting process mainly happens at the tool-nose radius due to the extremely shallow depth of the cut. This paper provides a comprehensive and systematic analysis of this issue based on an evaluation of tool geometry in hard turning via finite element analysis (FEA) simulations and experiments. The effect of tool angles on cutting temperature in hard turning is analyzed. The impacts of cutting-edge angle, rake angle, inclination angle, and average local rake angle on the cutting temperature are investigated via central composite design (CCD). The simulated results and the empirically measured cutting temperature exhibit comparable patterns, with a minor 2% difference. Increasing the cutting-edge angle, negative rake angle and negative inclination angle enhances the local negative rake angles of the cutting-edge elements at the tool-nose radius involved in the cutting process. Notably, the most important component influencing cutting temperature in hard turning is the inclination angle, as opposed to normal turning, where the rake angle dominates the heat generation. Following this is the cutting-edge angle and the rake angle, which each contribute 40.75%, 32.39%, and 7.03%. These findings could enhance the application of the hard-turning technique by improving tool life and surface quality by focusing on optimizing the inclination angle.

Keywords: cutting temperatures; tool geometry; hard turning

Academic Editor: Manoj Gupta

Received: 18 December 2024
Revised: 7 January 2025
Accepted: 16 January 2025
Published: 20 January 2025

Citation: Minh Duc, P.; Hieu Giang, L.; Nguyen, V.T. Analyzing Cutting Temperature in Hard-Turning Technique with Standard Inserts Through Both Simulation and Experimental Investigations. *Appl. Sci.* **2025**, *15*, 983. https://doi.org/10.3390/app15020983

1. Introduction

In recent years, there have been notable advancements in the machinability of hard processing materials. Machining high-hardness materials, or hard machining, offers numerous benefits, including cost savings, higher productivity rates, better surface quality, and the removal of deformities generated by cutting temperatures. Among them, hard turning is a technique for finishing machining parts made from high-hardness materials with a hardness greater than 45 HRC. Interestingly, hard turning can be performed without coolants, which is called dry hard turning. However, due to the single-point cutting contact, the elevated temperatures in the cutting zone can reduce tool life and deteriorate the machined surface due to thermal distortions [1].

During the hard machining process, the majority of the energy from cutting forces is converted into thermal energy [2,3]. There are many factors that influence thermal energy levels, including the physical and chemical properties of the workpiece and tool materials, cutting conditions, and tool geometry [4]. Moreover, this thermal energy is

mainly generated in three distinct zones: the primary zone, where the workpiece material suffers plastic deformation; the secondary zone, arising from friction between the tool and the chip; and the tertiary zone, caused by friction between the tool and the workpiece [5–7], as shown in Figure 1. Unfortunately, the elevated temperatures in the cutting zones, ranging from 800 to 1200 °C, reduce the tool's strength, hardness, and wear resistance [8].

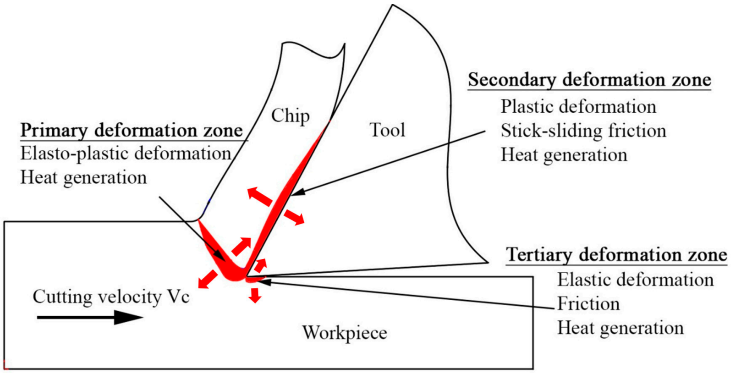

Figure 1. Mechanisms of heat generation and conduction in hard machining.

Moreover, the damage to the cutting tool due to the thermal issue also reduces the ability to control dimensional accuracy and maintain desired surface integrity, which leads to high machining costs and a reduction in product quality [9]. Therefore, many researchers have investigated the mechanism of heat generation and heat conduction to control its effects. Numerous researchers have employed actual cutting experiments or combined them with FEA simulations to evaluate the influence of input parameters on machining characteristics. The finite element method has been demonstrated as an effective approach for analyzing the chip-formation process and forecasting essential machining performance metrics, such as cutting temperatures, forces, and stresses. Hard turning differs significantly from conventional turning [10]. Hard turning is a finishing operation that involves high-speed cutting with a low feed rate and a shallow depth of cut not exceeding 0.2 mm [11–14]. Lezoglu et al. [15] and Mathivanan et al. [16] predicted cutting force and temperature distribution based on the FEA simulation models. They indicated that the tool should not be used near or over the diffusion and bonding limits of the materials employed in that particular tool grade.

Liu et al. [17] employed FEA simulations to examine the heat generated in the machining zones. Results from the FEA model were as accurate as those from experiments. The influence of workpiece hardness and cutting conditions on thermal generation during the hard turning of AISI H13-tool steel was investigated by Elsadek et al. [18]. According to the findings, workpiece hardness represented 63.77% of the cutting temperature, with cutting speed and feed rate following in at 16% and 4.78%, respectively. The depth of the cut factor has the least impact. Furthermore, Abrao et al. [19] discovered that while hard-turning AISI 52100 steel, cutting temperature rises with the increasing depth of cut, feed rate, cutting speed, and flank wear. Santhanakrishnan et al. [20] used the response surface methodology (RSM) to create a model to forecast workpiece temperature during the machining process of Al 6351. The results also showed that increasing the cutting speed causes higher cutting temperatures. Xu et al. [21] studied the cutting process of Inconel 718 by changing the rake angle. The cutting temperature when employing a tool with a negative rake angle is approximately 900 °C, whereas it is 750 °C for a neutral rake angle and 700 °C for a positive rake angle. Also, Saglam et al. [22] used carbide inserts to hard turn AISI 1040 steel (40 HRC) and examined the effects of rake and cutting-edge angles on cutting temperature. They discovered that a negative rake angle is typically used in hard turning to increase tool

strength and withstand high compressive pressures. Shah et al. [23] and Dutta et al. [24] investigated the impact of nose radii on the machining process of Ti- and Mg-based alloys. They both observed that larger nose radii lead to higher cutting temperatures, which can adversely affect tool life and surface integrity.

Despite there being many studies investigating the hard-turning process, the effects of the cutting tool's geometry are still rarely examined. Therefore, this study's goal is to use standard inserts to examine how the cutting tool's geometric factors affect cutting temperatures throughout the hard-turning process via both simulation and experiment methods. The impacts of cutting-edge angle, rake angle, inclination angle, and average local rake angle on the cutting temperature are examined. The study outcomes could outline more advantages of the applications of the hard-turning process. This study applies a "Hybrid Approach," which refers to the combined use of an analysis of tool geometry in hard turning, finite element analysis (FEA) simulations, and experimental methods, to investigate the effects of cutting-tool geometry on cutting temperature in hard turning. The methods are interactive and complementary in this study, providing robust insights into the hard-turning process, including an analysis of tool geometry, FEA simulations, and experimental validation.

2. Materials and Methods

2.1. The CCD Experimental Design

The central composite design (CCD) incorporates axial points ($-\alpha$ and $+\alpha$) to allow for quadratic modeling, enhancing the ability to detect curvature in the response surface used. This design ensures that the impacts of tool shape on machining responses can be precisely analyzed and optimized.

In Table 1, the experimental design is established based on the CCD method. The tool-geometry parameters investigated include the cutting-edge angle Kr, rake angle γ, and inclination angle λ, each varied at five levels ranging from $-\alpha$ to $+\alpha$. The ranges for the experimental parameters were selected based on the following considerations: tool manufacturers' recommendations and literature reviews on hard turning.

Table 1. Experimental design based on CCD.

Tool-Geometry Parameter	Unit	Levels				
		$-\alpha$	−1	0	+1	$+\alpha$
Kr	(°)	60	66	75	84	90
γ	(°)	−2	−3.6	−6	−8.4	−10
λ	(°)	−2	−3.6	−6	−8.4	−10

The encoded experimental factor matrix is presented in Table 2, detailing the combinations of tool-geometry parameters for each experimental run.

The cutting conditions were determined in accordance with the manufacturer's catalogue recommendations, as shown in Table 3.

Table 2. Coded experimental factor matrix.

No.	Factors			No.	Factors		
	K_r	γ	λ		K_r	γ	λ
1	+1	−1	−1	11	0	$-\alpha$	0
2	−1	−1	−1	12	0	$+\alpha$	0
3	+1	+1	−1	13	0	0	$-\alpha$
4	−1	+1	−1	14	0	0	$+\alpha$
5	+1	−1	+1	15	0	0	0
6	−1	−1	+1	16	0	0	0
7	+1	+1	+1	17	0	0	0
8	−1	+1	+1	18	0	0	0
9	$+\alpha$	0	0	19	0	0	0
10	$-\alpha$	0	0	20	0	0	0

Table 3. Fixed machining parameters in the study.

Cutting Speed v (m/min)	Feed Rate f (mm/rev)	Depth of Cut dw (mm)
150	0.08	0.2

2.2. Analysis of Tool Geometry in Hard Turning

Hard turning is typically a finishing process characterized by high cutting speeds, small depths of cut, and low feed rates [11–13]. The previously developed mathematical model of tool geometry in hard turning showed that the cutting action is confined to the tool-nose radius [25]. Therefore, the local tool-geometry parameters and the undeformed chip thickness of the tool-nose radius elements engaged in the cutting process are determined as shown in Figure 2, using the following input parameters: cutting-edge angle $K_r = 60°$, inclination angle $\lambda = -6°$, rake angle $\gamma = -6°$, tool-nose radius $r = 0.8$ mm, chamfer angle = $-25°$, and chamfer width = 1.5 mm. The equations of the proposed model are presented as [25]:

- The portion of the nose radius involved in the cutting process:

$$\theta_A = K_r - cos^{-1}\left(\frac{r - d_w}{r}\right)$$

$$\theta_C = K_r$$

$$\theta_D = K_r + sin^{-1}\left(\frac{f}{2r}\right)$$

$$\theta_B = K_r - tan^{-1}\left(\frac{rsin(K_r - \theta_A) - f}{r - d_w}\right)$$

- Local rake angle:

$$\gamma^j = tan^{-1}\left(sin\left(\frac{\pi}{2} - \theta^j\right)tan\gamma + cos\left(\frac{\pi}{2} - \theta^j\right)tan\lambda\right)$$

- Local undeformed chip thickness:

$$\text{Zone 1}: \ \theta_A \le \theta^j < \theta_B$$

$$t_1(\theta^j) = r - \frac{r - d_w}{\cos(K_r - \theta^j)}$$

$$\text{Zone 2}: \ \theta_B \le \theta^j \le \theta_D$$

$$t_2(\theta^j) = r - \sqrt{r^2 + f^2 - 2rf\cos\left(\theta^j + \frac{\pi}{2} - K_r - \sin^{-1}\left(\frac{f}{r}\sin\left(\theta^j + \frac{\pi}{2} - K_r\right)\right)\right)}$$

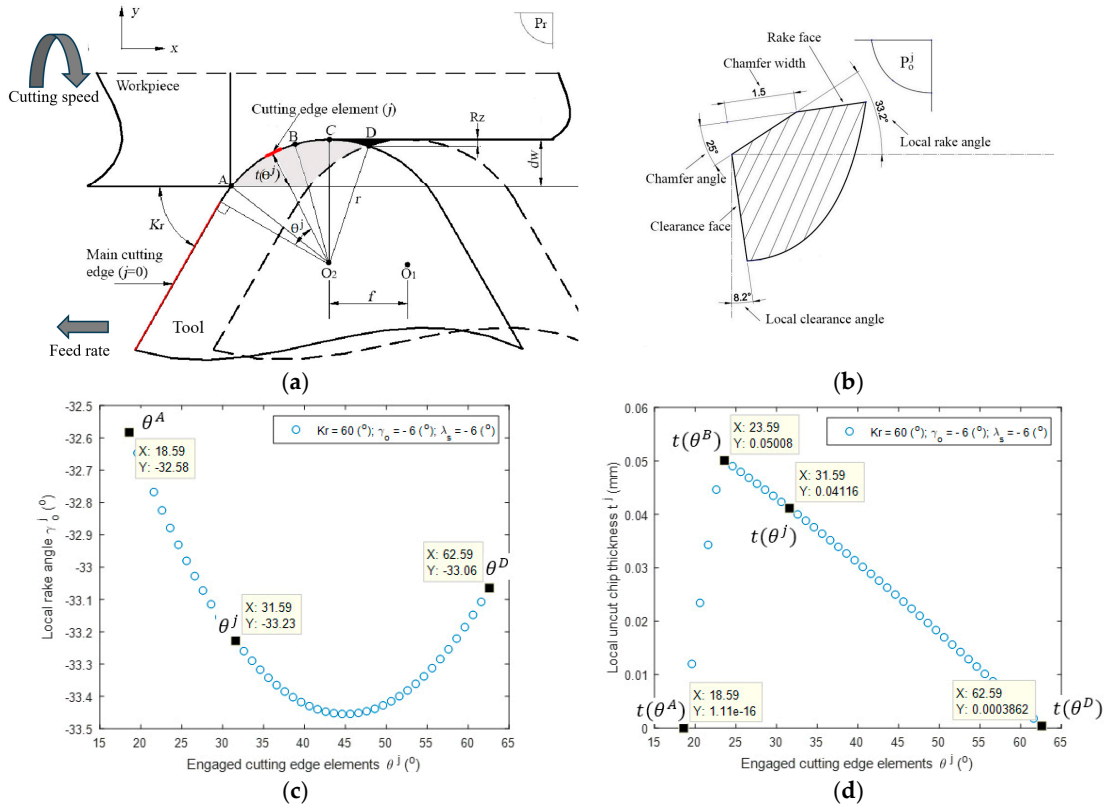

Figure 2. (**a**) Hard-turning configuration; (**b**) Cutting-edge element geometry j at $\theta^j = 31.59°$; (**c**) Local rake angles; (**d**) Local uncut chips.

From Figure 2c,d, the cutting process occurs from $\theta^A = 18.59°$ to $\theta^D = 62.59°$. At the cutting-edge element $\theta^D = 23.59°$, the largest uncut chip thickness $t(\theta^D) = 0.05$ (mm).

2.3. FEM Simulation

In this study, the FEM method is used to simulate the hard turning of AISI H13 hardened steel (52 HRC) using a TiN-coated ceramic tool. DEFORM 3D software (version 11), which employs an implicit Lagrangian computational technique, is used for FEM analysis. The workpiece is modeled as a plastic-behavior material, represented as a curved structure with a diameter of 53 mm and an arc angle of 20°, and it is meshed around 32,000 to 60,000 tetrahedral elements, depending on the feeding rate.

The mesh's minimum element size was set to 25% of the feed value [26,27]. DEFORM-3D's default remeshing functionality was used to ensure that the mesh within the critical area retained an acceptable number of elements while new chips were created during the manufacturing process. In addition, a 7:1 ratio was maintained between the greatest and smallest element sizes in the workpiece mesh, as seen in Figure 3. This arrangement ensures that the solid elements used in the material removal procedure are seven-times smaller than the surrounding elements. In the finite element simulation, the tool insert designated by ISO code TNGA160408S01525 was modeled as a rigid body and discretized into approximately 45,000 tetrahedral elements. To improve computational accuracy, the region at the tool tip that contacts the workpiece was improved using a 4:1 size ratio, which was consistent with the workpiece meshing approach. Furthermore, DEFORM-3D's default remeshing functionality was used to ensure that the mesh within the critical area retained

an acceptable number of elements while new chips were created during the manufacturing process. To simulate the cutting process, the workpiece model was constrained in position, while the cutting tool was permitted to move along the defined cutting trajectory. There were 10,000 simulation steps.

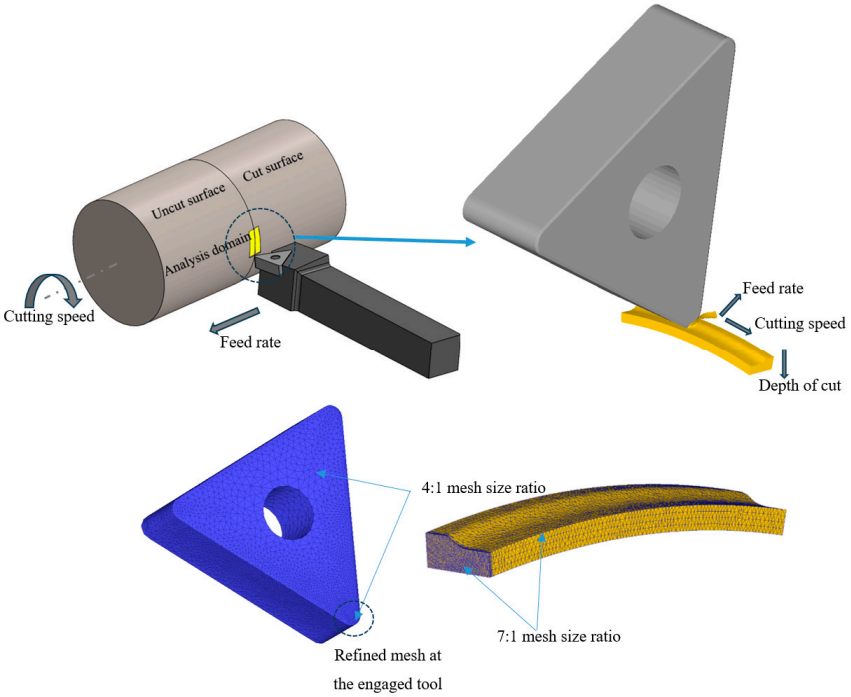

Figure 3. Set up of hard-turning simulation process.

The machining process was conducted at an ambient temperature of 27 °C, employing a convection coefficient of 0.02 N/s/mm/°C. A shear friction factor of 0.6 was applied at the interface between the tool and the workpiece [28], and the heat-transfer coefficient was specified as 45 N/s/mm/°C without the use of any coolant. The flow stress of the material is influenced by temperature T, strain $\bar{\varepsilon}$, and strain rate $\dot{\bar{\varepsilon}}$; therefore, it can be modeled using the following Johnson–Cook equation:

$$\overline{\sigma} = (\mathrm{A} + \mathrm{B}\bar{\varepsilon}\mathrm{n})\left(1 + \mathrm{C}\ln\left(\frac{\dot{\bar{\varepsilon}}}{\dot{\bar{\varepsilon}}_o}\right)\right)\left(1 - \left(\frac{T - T_o}{T_m - T_o}\right)^m\right)$$

where $\overline{\sigma}$ is flow stress, $\bar{\varepsilon}$ is equivalent plastic strain, $\dot{\bar{\varepsilon}}$ is the strain rate, $\dot{\bar{\varepsilon}}_o$ is the reference strain rate, T is temperature, T_o is room temperature, T_m is the melting temperature, A is the yield-stress constant, B is the strain-hardening coefficient, n is the strain-hardening index, C is strain-rate dependence coefficient, and m is the temperature-dependence coefficient. The Johnson–Cook model constants for AISI H13 follows Zhang et al.'s report [29], as shown in Table 4.

Table 4. Johnson–Cook model constants for AISI H13 (52HRC) [29].

A (MPa)	B (MPa)	n	C	m	$\dot{\bar{\varepsilon}}_o$ (1/s)	T_o (°C)	T_m (°C)
908.54	321.39	0.278	0.028	1.18	1.0	27	1475

The tool-workpiece system was defined in such a way that the problem was simplified in terms of the analysis domain. The point of this simplification is to achieve reasonable simulation times. First, the tool-holder model was eliminated from the tool assembly and

only the insert model was used. Furthermore, the round steel-bar model was converted to an arc-shaped part. The arc has a 20° angle and belongs to a circle with a diameter of 53 mm. In addition, the workpiece was designed partially cut based on the used depth of the cut, to reduce computational costs.

2.4. Experimental Procedure

The experimental procedure was conducted under conditions similar to those used in the simulations. Hard-turning operations were conducted using a BOEHRINGER DUS-400ti CNC lathe, as depicted in Figure 4. The workpieces were made of AISI H13 hardened steel (52 HRC), measuring 53 mm in diameter and 80 mm in length.

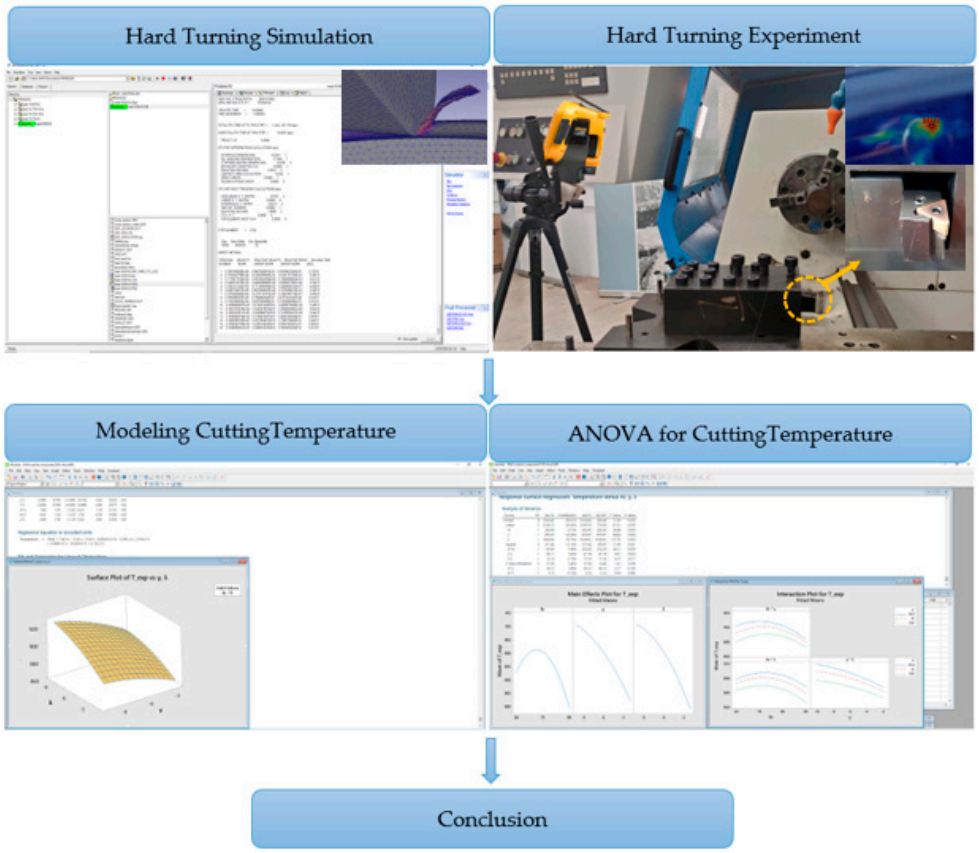

Figure 4. Flow diagram of the hard-turning research process.

The thermo-mechanical characteristics of the workpiece and the tool are presented in Table 5. The titanium nitride (TiN)-coated ceramic inserts employed had an ISO designation of TNGA160408S01525 and were secured on a tool holder designated as PTGNR 1616H 16. This configuration of the insert and tool holder provided cutting-edge angle $K_r = 91°$, rake angle $\gamma = -6°$, and inclination angle $\lambda = -6°$. Sandvik inserts and tool holders were employed in the experimental setup. To facilitate adjustments in tool angles, a specialized tool-post system was designed using SolidWorks 2021 software. This system was fabricated on a DMG MORI DMU65 monoBLOCK five-axis milling center and subsequently evaluated using a Hexagon GLOBAL Classic coordinate measuring machine (CMM).

Table 5. Thermo-mechanical characteristics of the tool and the workpiece.

Thermo-Mechanical Properties	AISI H13	Ceramic Tool	TiN Coating
Young's Modulus (GPa)	211	145	-
Poisson ratio	0.28	0.22	0.25
Density (kg/m^3)	7800	3500	4650
Thermal conductivity (W/m·°C)	37	24	23.5
Hardness (HV)	544	-	2300

Many techniques can be used to measure temperature during the machining process, which depend on the specific conditions under which measurements are conducted [30–32]. A FLUKE Ti400 infrared (IR) thermal imager was used in this investigation to determine the temperature at the tool–chip contact zone. This temperature measurement system automatically corrected for atmospheric transmission based on input parameters such as the distance to the object, atmospheric temperature, and relative humidity. The captured thermal images were then analyzed using FLUKE's SmartView analysis software (version 4.4). Cutting temperature measurements were conducted three times for each set of tool-structure parameters to account for variability and ensure reliability. The reported temperature values are the averages of these repeated measurements, and the standard deviations were within acceptable limits, indicating good repeatability of the results.

3. Results and Discussion

The central composite design (CCD) and the experimental results are presented in Table 6. Analysis of variance (ANOVA) is a statistical technique employed to evaluate the impact of input variables on the output responses of a technical process with a 95% confidence level. In other words, a *p*-value of less than 0.05 indicates that the model is statistically significant. Another essential statistic is the coefficient of correlation (R^2), which measures the model's degree of fit. Notably, the simulation findings and empirically measured cutting temperature show similar patterns, with only a 2% difference, indicating comparable results. As shown in Table 6, the simulated temperature values are all higher than the experimental measurement values. This discrepancy arises because the infrared thermal imager used in the experiments captures surface temperatures, whereas the simulation estimates the internal cutting-zone temperature (at the interface between the tool and the chip). This is because the internal zones naturally experience higher temperatures than those visible externally. The average local rake angle and cutting temperature results will be further analyzed in the following figures.

Figure 5 presents the cutting process in the hard-turning method. The simulation results demonstrated that the main cutting edge does not participate in the cutting action. The cutting process occurs exclusively at the tool-nose radius. Moreover, the chip makes contact only with the chamfered face of the cutting edge. The data obtained from the further experiments results could reveal more information.

Table 7 shows the ANOVA results for the average local rake angle. The results indicate that the most significant factor is the inclination angle, accounting for 65.84%, followed by the rake angle, contributing 31.43%. The cutting-edge angle only contributes 0.98% to the average local rake angle. Therefore, optimizing the hard-turning process should concentrate on modifying the inclination angle and rake angle. The cutting-edge angle could be ignored as its effect is minor. The main effect plots for the average local rake angle are presented in Figure 6. Increasing the negative rake and inclination angles leads to a greater negative local rake angle of the cutting-edge elements at the tool-nose radius engaged in the cutting process.

Figure 7 presents the temperature distributions at the chip–tool interface, as determined through 3D FEM simulation. The cutting temperature is highest at the contact area between the chip and the tool, consistent with the findings of Hao et al. [33]. The cutting temperature could reach a range of 800–900 °C, which is close to the experimental results shown in Table 5. This is due to the heat generated in the primary shear-deformation zone being transferred to the chip and the heat produced by friction between the chip and the chamfered face. Moreover, as shown in Figure 5, the contact type is only a point at the small cutting depth in the hard-turning process rather than the facial type at the higher cutting depth in the conventional machining process.

Table 8 displays the ANOVA for experimental cutting temperature. The results show that inclination angle is the dominant contributor to cutting temperature, accounting for 40.75% of total variability, whereas the rake angle has a modest influence, which accounts for 32.39% of the total variability. The cutting-edge angle has a lower level of contribution (7.03%), and all interaction effects are insignificant. Notably, all interaction effects are insignificant because the contribution values of two-way interaction are too small, as shown in Table 8. These results are consistent with the analysis of tool geometry in hard turning, which demonstrated that the inclination angle has the most significant influence on the local rake angle. The quadratic model for cutting temperature (1) with R^2= 95.2% indicates a high degree of concordance between the predicted and experimental values, as shown in Figure 8. The regression equation for the cutting temperature be presented as follows:

$$\begin{aligned} T\_exp = {} & 510.9 + 9.07\,Kr - 10.87\,\gamma - 3.74\,\lambda - 0.0619\,Kr \times Kr - 0.246\,\gamma\times\gamma - 0.340 \\ & \lambda \times \lambda + 0.0752\,Kr \times \gamma - 0.0405\,Kr \times \lambda + 0.195\,\gamma\times\lambda \end{aligned} \quad (1)$$

Table 6. Central composite design (CCD) and experimental results.

No.	Cutting-Edge Angle K_r (°)	Rake Angle γ (°)	Inclination Angle λ (°)	Average Local Rake Angle γ_ave (°)	Simulated Temperature T_sim (°C)	Experimental Temperature T_exp (°C)
1	84	−3.6	−3.6	−29.7	888	868
2	66	−3.6	−3.6	−30	900	881
3	84	−8.4	−3.6	−31.7	905	887
4	66	−8.4	−3.6	−33.2	914	892
5	84	−3.6	−8.4	−33.9	912	895
6	66	−3.6	−8.4	−33.3	911	890
7	84	−8.4	−8.4	−35.9	922	904
8	66	−8.4	−8.4	−36.5	939	920
9	90	−6.0	−6.0	−32.4	903	880
10	60	−6.0	−6.0	−33.2	916	894
11	75	−2.0	−6.0	−30.9	903	884
12	75	−10.0	−6.0	−35.3	927	910
13	75	−6.0	−2.0	−29.9	902	882
14	75	−6.0	−10.0	−36.3	927	909
15	75	−6.0	−6.0	−33.1	919	900
16	75	−6.0	−6.0	−33.1	922	902
17	75	−6.0	−6.0	−33.1	921	903
18	75	−6.0	−6.0	−33.1	920	900
19	75	−6.0	−6.0	−33.1	919	898
20	75	−6.0	−6.0	−33.1	920	901

Table 7. ANOVA result for average local rake angle.

Source	DF	Seq SS	Contribution	Adj SS	Adj MS	F-Value	*p*-Value
Model	9	73.7959	99.98%	73.7959	8.1995	6783.94	0.000
Linear	3	72.5213	98.26%	72.5213	24.1738	20,000.32	0.000
Kr	1	0.7243	0.98%	0.7243	0.7243	599.22	0.000
γ	1	23.1987	31.43%	23.1987	23.1987	19,193.58	0.000
λ	1	48.5984	65.84%	48.5984	48.5984	40,208.15	0.000
Square	3	0.1496	0.20%	0.1496	0.0499	41.26	0.000
Kr × Kr	1	0.1483	0.20%	0.1426	0.1426	118.01	0.000
γ× γ	1	0.0006	0.00%	0.0007	0.0007	0.60	0.458
λ× λ	1	0.0007	0.00%	0.0007	0.0007	0.60	0.458
2-Way Interaction	3	1.1250	1.52%	1.1250	0.3750	310.26	0.000
Kr × γ	1	0.7200	0.98%	0.7200	0.7200	595.70	0.000
Kr × λ	1	0.4050	0.55%	0.4050	0.4050	335.08	0.000
γ× λ	1	0.0000	0.00%	0.0000	0.0000	0.00	1.000
Error	10	0.0121	0.02%	0.0121	0.0012		
Lack-of-Fit	5	0.0121	0.02%	0.0121	0.0024		
Pure Error	5	0.0000	0.00%	0.0000	0.0000		
Total	19	73.8080	100.00%				

Table 8. ANOVA result for experimental cutting temperature.

Source	DF	Seq SS	Contribution	Adj SS	Adj MS	F-Value	*p*-Value
Model	9	2736.17	95.20%	2736.17	304.02	22.06	0.000
Linear	3	2304.11	80.17%	2304.11	768.04	55.72	0.000
Kr	1	202.04	7.03%	202.04	202.04	14.66	0.003
γ	1	930.89	32.39%	930.89	930.89	67.54	0.000
λ	1	1171.18	40.75%	1171.18	1171.18	84.97	0.000
Square	3	394.68	13.73%	394.68	131.56	9.55	0.003
Kr × Kr	1	319.34	11.11%	352.95	352.95	25.61	0.000
γ× γ	1	21.68	0.75%	28.12	28.12	2.04	0.184
λ× λ	1	53.67	1.87%	53.67	53.67	3.89	0.077
2-Way Interaction	3	37.38	1.30%	37.38	12.46	0.90	0.473
Kr × γ	1	21.13	0.74%	21.12	21.12	1.53	0.244
Kr × λ	1	6.12	0.21%	6.12	6.12	0.44	0.520
γ× λ	1	10.13	0.35%	10.13	10.13	0.73	0.411
Error	10	137.83	4.80%	137.83	13.78		
Lack-of-Fit	5	122.49	4.26%	122.49	24.50	7.99	0.020
Pure Error	5	15.33	0.53%	15.33	3.07		
Total	19	2874.00	100.00%				

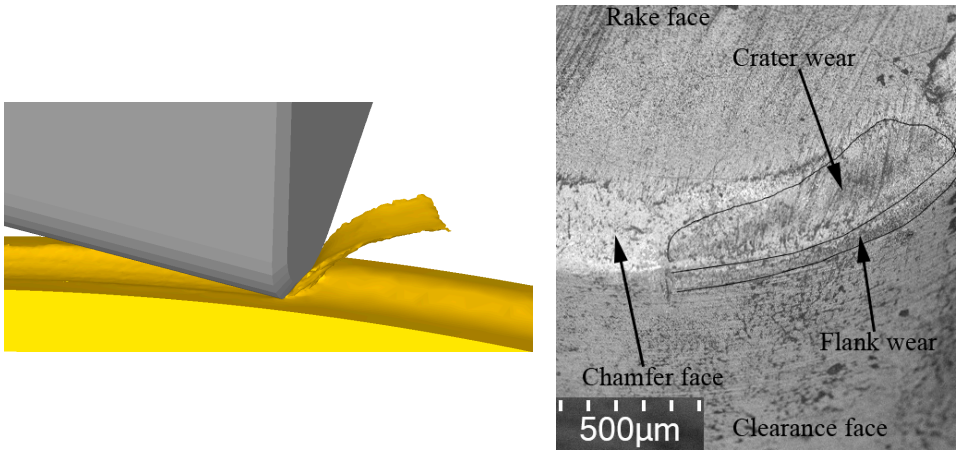

(**a**) (**b**)

Figure 5. The cutting process at the tool-nose radius in hard turning as determined from (**a**) simulation and (**b**) experimental results.

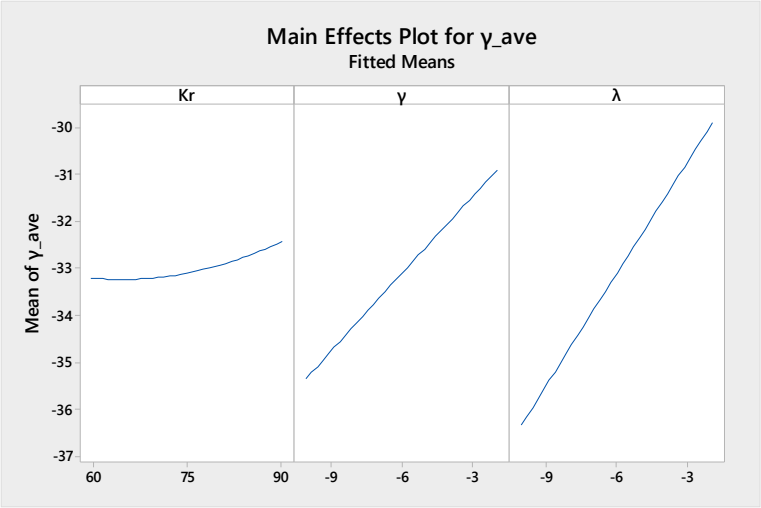

Figure 6. Main effect plots for average local rake angle.

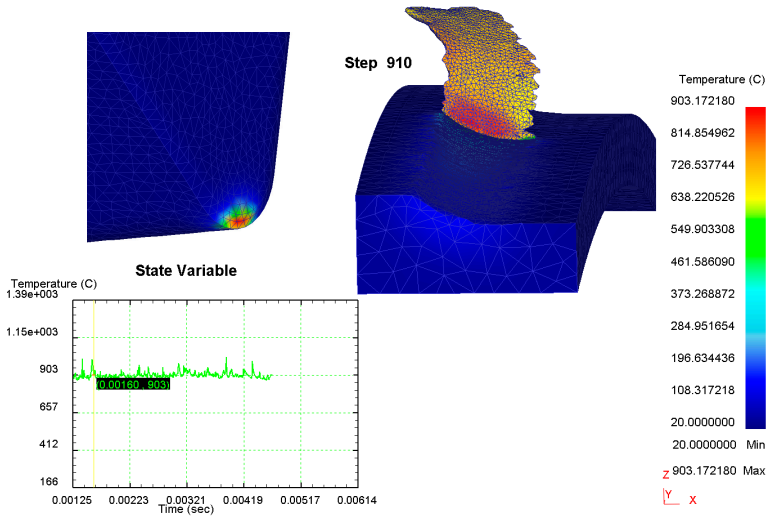

Figure 7. Temperature distributions at the chip–tool interface, as determined through 3D finite element modeling (FEM).

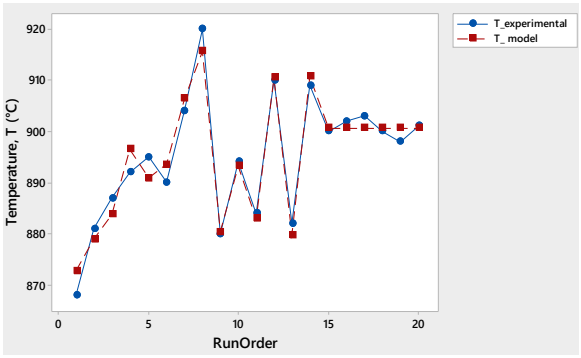

Figure 8. Comparison of measured and predicted temperatures.

The main effect plots for the simulation and experimental cutting temperature are shown in Figures 9 and 10. They both indicate that increasing the negative rake angle and negative inclination angle leads to a rise in cutting temperature. The reason is when the negative inclination angle and rake angle are increased, the local rake angle becomes more negative. This results in increased friction at the contact surface between the chip and the chamfered face of the tool, as well as greater material deformation in the primary and secondary shear zones, thereby raising the cutting temperature. Figure 11 presents the relationship between the rake angle, inclination angle, and cutting temperature, which is consistent with the results in Figures 9 and 10. This figure also reveals that increasing the negative rake angle and negative inclination angle raises the cutting temperature. Interestingly, Figure 8 presents the comparison of measured and predicted temperatures of the hard-turning process. The results from the FEM simulation are mostly consistent with the calculated results, indicating the reliability of the model.

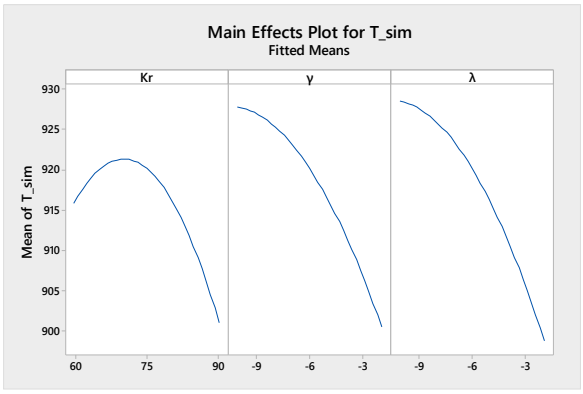

Figure 9. Main effect plots for FEM cutting temperature.

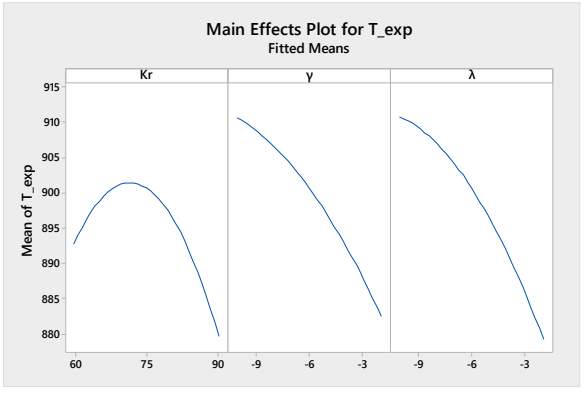

Figure 10. Main effect plots for experimental cutting temperature.

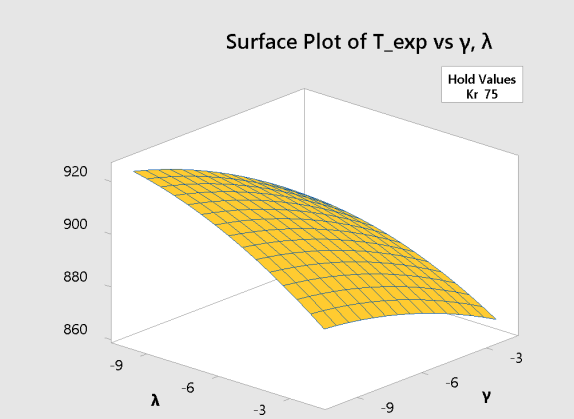

Figure 11. Cutting temperature vs. rake and inclination angles' response surface in hard turning.

4. Conclusions

In this study, the effect of insert-angle factors on cutting temperature in the hard-turning process is explored using a combined approach. Several conclusions have been determined, as follows:

- The cutting temperature from the experiment and the simulation results have consistent values, reaching about 900 °C. The difference in the experiment and simulation results is small—approximately 2%.
- Only the tool-nose radius cuts during the hard-turning operation, and the chip makes contact with the cutting edge's chamfered face. At each cutting point, the local tool-geometry parameters and the thickness of the undeformed chip change, and the local rake angle becomes noticeably negative.
- Increasing the negative rake angle and negative inclination angle improves the local negative rake angle of the cutting-edge elements at the tool-nose radius during the hard-turning process, accounting for 65.84% and 31.43%, respectively.
- The most significant factor influencing cutting temperature is the inclination angle, which accounts for 40.75% of the total variability. The rake angle has a smaller effect, accounting for 32.39% of the total variability, and the cutting-edge angle accounts for 7.03%.

The interactions between the components are not significant. Increasing the negative rake angle and negative inclination angle raises the cutting temperature. This study's findings could bring about additional benefits for applications of the hard-turning technique.

Author Contributions: Conceptualization, P.M.D. and L.H.G.; methodology, P.M.D.; software, V.T.N.; validation, P.M.D., L.H.G. and V.T.N.; formal analysis, P.M.D.; investigation, P.M.D.; resources, P.M.D.; data curation, P.M.D.; writing—original draft preparation, P.M.D.; writing—review and editing, P.M.D., L.H.G. and V.T.N.; visualization, V.T.N.; supervision, L.H.G.; project administration, P.M.D.; funding acquisition, P.M.D. All authors have read and agreed to the published version of the manuscript.

Funding: This research received no external funding.

Institutional Review Board Statement: Not applicable.

Informed Consent Statement: Not applicable.

Data Availability Statement: The data presented in this study are available on request from the corresponding author. The data are not publicly available due to privacy.

Acknowledgments: We are grateful to Ho Chi Minh University of Technology and Education for providing the facilities for us to carry out this study.

Conflicts of Interest: The authors declare no conflicts of interest.

References

1. Haq, A.N.; Tamizharasan, T. Investigation of the effects of cooling in hard turning operations. *Int. J. Adv. Manuf. Technol.* **2006**, *30*, 808–816.
2. Abukhshim, N.A.; Mativenga, P.T.; Sheikh, M.A. Heat generation and temperature prediction in metal cutting: A review and implications for high-speed machining. *Int. J. Mach. Tools Manuf.* **2006**, *46*, 782–800. [CrossRef]
3. Silva, M.B.; Wallbank, J. Cutting temperature: Prediction and measurement methods—A review. *J. Mater. Process. Technol.* **1999**, *88*, 195–202. [CrossRef]
4. Hao, G.; Liu, Z. The heat partition into cutting tool at tool-chip contact interface during cutting process: A review. *Int. J. Adv. Manuf. Technol.* **2020**, *108*, 393–411. [CrossRef]
5. Bhirud, N.L.; Gawande, R.R. Measurement and prediction of cutting temperatures during dry milling: Review and discussions. *J. Braz. Soc. Mech. Sci. Eng.* **2017**, *39*, 5135–5158. [CrossRef]
6. Grzesik, W. Heat in metal cutting. In *Advanced Machining Processes of Metallic Materials*; Elsevier: Amsterdam, The Netherlands, 2017; pp. 163–182.
7. Trent, E.M.; Wright, P.K. Heat in metal cutting. In *Metal Cutting*; Butterworth-Heinemann: Oxford, UK, 2000; pp. 97–131.
8. Wang, Y.; Wang, Z.; Ni, P.; Wang, D.; Lu, Y.; Lu, H.; Guo, S.; Chen, Z. Experimental and numerical study on regulation of cutting temperature during the circular sawing of 45 steel. *Coatings* **2023**, *13*, 758. [CrossRef]
9. Puls, H.; Klocke, F.; Veselovac, D. FEM-based prediction of heat partition in dry metal cutting of AISI 1045. *Int. J. Adv. Manuf. Technol.* **2016**, *86*, 737–745. [CrossRef]
10. Davim, J.P. *Machining of Hard Materials*; Springer: London, UK, 2011.
11. Dessoly, V.; Melkote, S.N.; Lescalier, C. Modeling and verification of cutting tool temperature in rotary tool turning of hardened steels. *Int. J. Mach. Tools Manuf.* **2004**, *44*, 1463–1470. [CrossRef]
12. Diniz, A.E.; Oliveira, A.J. Hard turning of interrupted surfaces using CBN tool. *J. Mater. Process. Technol.* **2008**, *195*, 275–281. [CrossRef]
13. Grezesik, W. Influence of tool wear on surface roughness in HT using differently shaped ceramic tools. *Wear* **2008**, *265*, 327–335. [CrossRef]
14. Bartarya, G.; Choudhury, S.K. State of the art in hard turning. *Int. J. Mach. Tools Manuf.* **2012**, *53*, 1–14. [CrossRef]
15. Lazoglu, I.; Altintas, Y. Prediction of tool and chip temperature in continuous and interrupted machining. *Int. J. Mach. Tools Manuf.* **2002**, *42*, 1011–1022. [CrossRef]
16. Mathivanan, A.; Sudeshkumar, M.P.; Ramadoss, R.; Ezilarasan, C.; Raju, G.; Jayaseelan, V. Finite element simulation and regression modeling of machining attributes on turning AISI 304 stainless steel. *Manuf. Rev.* **2021**, *8*, 24. [CrossRef]
17. Liu, Z.; Yue, C.; Li, X.; Liu, X.; Liang, S.Y.; Wang, L. Research on tool wear based on 3D FEM simulation for milling process. *J. Manuf. Mater. Process.* **2020**, *4*, 121. [CrossRef]
18. Elsadek, A.A.; Gaafer, A.M.; Mohamed, S.S. Prediction and optimization of cutting temperature on hard turning. *SN Appl. Sci.* **2020**, *2*, 540. [CrossRef]
19. Abrão, A.M.; Aspinwall, D.K.; Wise, M.H.L. *Tool Life and Workpiece Surface Integrity Evaluations when Machining Hardened AISI H13 and AISI E52100 Steels with Conventional Ceramic and PCBN Tool Materials*; Society of Manufacturing Engineers: Southfield, MI, USA, 1995; pp. 1–7.
20. Santhanakrishnan, M.; Sivasakthivel, P.S.; Sudhakaran, R. Modeling of geometrical and machining parameters on temperature rise while machining Al 6351 using response surface methodology and genetic algorithm. *J. Braz. Soc. Mech. Sci. Eng.* **2017**, *39*, 487–496. [CrossRef]
21. Xu, D.; Ding, L.; Liu, Y.; Zhou, J.; Liao, Z. Investigation of the Influence of Tool Rake Angles on Machining of Inconel 718. *J. Manuf. Mater. Process.* **2021**, *5*, 100. [CrossRef]
22. Saglam, H.; Unsacar, F.; Yaldiz, S. Investigation of the effect of rake angle and approaching angle on main cutting force and tool tip temperature. *Int. J. Mach. Tools Manuf.* **2006**, *46*, 132–141. [CrossRef]
23. Shah, D.; Bhavsar, S. Effect of tool nose radius and machining parameters on cutting force, cutting temperature and surface roughness—An experimental study of Ti-6Al-4V (ELI). Mater. *Today Proc.* **2020**, *22*, 1977–1986. [CrossRef]
24. Dutta, S.; Narala, S.K.R. Effect of tool nose radius in turning of novel Mg alloy. *Mater. Today Proc.* **2021**, *38*, 2675–2679. [CrossRef]
25. Duc, P.M.; Dai, M.D.; Giang, L.H. Modeling and optimizing the effects of insert angles on hard turning performance. *Math. Probl. Eng.* **2021**, *2021*, 9924427. [CrossRef]
26. Tzotzis, A.; Garcia-Hernandez, C.; Talón, J.L.H.; Kyratsis, P. Influence of the nose radius on the machining forces induced during AISI-4140 hard turning: A CAD-based and 3D FEM approach. *Micromachines* **2020**, *11*, 798. [CrossRef] [PubMed]
27. Tzotzis, A.; Garcia-Hernandez, C.; Talón, J.L.H.; Kyratsis, P. 3D FE Modelling of machining forces during AISI 4140 hard turning. Strojniški Vestn. *J. Mech. Eng.* **2020**, *66*, 467–478. [CrossRef]

28. Haglund, A.J.; Kishawy, H.A.; Rogers, R.J. An exploration of friction models for the chip-tool interface using an Arbitrary Lagrangian-Eulerian finite element model. *Wear* **2008**, *265*, 452–460. [CrossRef]
29. Zhang, S.; Li, B.; Li, J.; Man, J. Effects of constitutive model parameters on finite element simulation process for hard milling of AISI H13 steel. *MM Sci. J.* **2021**, *2021*, 5234–5240. [CrossRef]
30. Davies, M.; Ueda, T.; M'Saoubi, R.; Mullany, B.; Cooke, A. On the measurement of temperature in material removal processes. *CIRP Ann.* **2007**, *56*, 581–604. [CrossRef]
31. Weng, J.; Saelzer, J.; Berger, S.; Zhuang, K.; Bagherzadeh, A.; Budak, E.; Biermann, D. Analytical and experimental investigations of rake face temperature considering temperature-dependent thermal properties. *J. Mater. Process. Technol.* **2023**, *314*, 117905. [CrossRef]
32. Guimaraes, B.M.P.; Fernandes, C.M.D.S.; de Figueiredo, D.A.; da Silva, F.S.C.P.; Miranda, M.G.M. Cutting temperature measurement and prediction in machining processes: Comprehensive review and future perspectives. *Int. J. Adv. Manuf. Technol.* **2022**, *120*, 2849–2878. [CrossRef]
33. Hao, G.; Tang, A.; Zhang, Z.; Xing, H.; Xu, N.; Duan, R. Finite element simulation of orthogonal cutting of H13-hardened steel to evaluate the influence of coatings on cutting temperature. *Coatings* **2024**, *14*, 293. [CrossRef]